Applied Thermal Engineering 117 (2017) 782–798

Contents lists available at ScienceDirect

Applied Thermal Engineering

journal homepage: www.elsevier.com/locate/apthermeng

Research Paper

Experimental study of heat transfer and start-up of loop heat pipe with multiscale porous wicks

Xianbing Ji [a], Ye Wang [a], Jinliang Xu [a,*], Yanping Huang [b]

[a] The Beijing Key Laboratory of Multiphase Flow and Heat Transfer, North China Electric Power University, Beijing 102206, PR China
[b] CNNC Key Laboratory on Nuclear Reactor Thermal Hydraulics Technology, Nuclear Power Institute of China, Chengdu 610213, PR China

HIGHLIGHTS

- A loop heat pipe with composite multiscale wicks was designed and investigated.
- Composite wicks can shorten start-up time and decrease start-up temperature.
- Achieve a synergy between thermal conductivity and thermal insulation.
- Nucleate boiling and film evaporation regions were observed.

ARTICLE INFO

Article history:
Received 19 October 2016
Revised 18 January 2017
Accepted 24 January 2017
Available online 27 January 2017

Keywords:
Multiscale
Loop heat pipe
Composite porous wick
Synergy

ABSTRACT

A loop heat pipe (LHP) with composite multiscale porous wicks was designed and investigated. The focus was on heat transfer and start-up characteristics. Three layers of wick were used to form the composite wicks. The primary layer was sintered on the evaporator wall using copper powder with different average particle diameters (d_p = 13, 37, 88, and 149 μm) to form a groove multiscale wick. The second layer was laid on top of the first one by a second sintering. The third layer was made of absorbent wool with excellent thermal insulation. A series of experiments were performed to study the effects of various parameters, including wick structures, tilt angles (θ = −90°, 0°, and 90°), liquid filling ratios (38.5–64.1%), liquid line lengths, and heating power. Compared with conventional monoporous wicks, the composite multiscale porous wicks shortened the start-up time, decreased the wall temperature, and suppressed the temperature instability of the LHP. At a heat load of 200 W, the LHP with composite wicks could reach a heat flux of 40 W/cm^2 for the anti-gravity operation, under which the wall temperature was only 63 °C. Some reasons that accounted for performance improvement were as follows: the porous groove wall increased the surface area and multiscale structures realized a successful synergy between vapor release and liquid supply, large pores for vapor release, and small pores for liquid suction. In addition, a synergy between thermal conductivity and insulation was achieved, which ensured a high thermal conductivity for the primary layer wick and a good thermal insulation for the entire wick. This greatly reduced the heat leakage from the evaporator to the compensation chamber.

1. Introduction

With the development of science and technology, infrared detector arrays, solid lasers, high-performance microprocessors, and other optical/microelectronic chip devices are becoming smaller and more integrated. In these devices, a considerable amount of heat is produced within a small space, and it is difficult to dissipate this heat by natural or forced convection. Loop heat pipe (LHP), as a two-phase heat transfer device, plays a vital role in heat dissipation and has been widely used in energy applications, spacecraft, electronics device cooling, and commercial radiators [1,2]. After Gerasimov and Maydanik patented LHP in 1972 [3], many scholars have conducted a significant amount of research on LHP [4,5].

In LHP, porous wicks are the core components. They provide a capillary force for the circulation of the working fluid and a liquid flow path and place for the phase change heat transfer. Thus, the heat transfer and start-up characteristics of the LHP are closely related to the structures of porous wicks. So far, various wicks such as groove wicks [6], metal mesh wicks [7,8], polymer wicks [9,10], ceramics wicks [11], and metal powder sintered wicks (including

* Corresponding author.
E-mail address: xjl@ncepu.edu.cn (J. Xu).

http://dx.doi.org/10.1016/j.applthermaleng.2017.01.084
1359-4311/

Nomenclature

A	heater area on the wall, m^2
c_p	specific heat capacity, J/(kg K)
D_c	compensation chamber diameter, m
D_e	evaporator diameter, m
D_{ei}	wick layer diameter, m
d_e	effective pore diameter, m
d_p	particle diameter, m
ΔH	anti-gravity height, m
h	groove depth, m
L_l	liquid line length, m
m	mass flow rate, kg/s
p	groove wall width, m
Δp	pressure drop, Pa
Q	heat load, W
q	heat flux, W/cm^2
R	thermal resistance, K/W
r	latent heat vaporization, J/kg
T	temperature, K
t	time, s
w	groove width, m

Greek symbols

α	contact angle, °
β	heat leakage percentage
h	heat
δ	thickness of porous covers, m
ε	porosity of wick
ϕ	liquid filling ratio
μ	viscosity, kg/(m s)
θ	tilt angles of LHP, °
ρ	density, kg/m^3
σ	surface tension force, N/m

Subscripts

air	air
C	center wall of evaporator
Cin	condenser inlet
Cout	condenser outlet
cond	condenser
CP	compensation chamber
cpr	capillary pressure
CPin	compensation chamber inlet
*C*1∼*C*4	location on condenser tube line
Eout	vapor outlet port
e	evaporator
f	flow
g	gravity
l	liquid
L	loop heat pipe
t	total
w	wick
V	vapor tube line
v	vapor
vap	vaporization
1∼8	location on evaporator wall

stainless steel wicks [12], nickel wicks [13], and copper wicks [14]) have been studied and applied to the LHP [15].

However, the above mentioned studies mostly employ monoporous wicks, also called single-scale porous wicks. These wicks cannot handle high heat flux owing to the conflict between vapor release and liquid suction. According to Meléndez and Reyes [16],

$$m_v = \frac{\pi}{128}\left(\frac{\rho_v \sigma}{\mu_v}\right)\left(\frac{\varepsilon d_e^3}{\delta}\right) \tag{1}$$

where m_v is the mass flow rate of vapor; ρ_v, σ, μ_v, and ε are the vapor density, surface tension, viscosity, and porosity, respectively; δ is the wick thickness, and d_e is the effective pore diameter. Large mass flow rate of vapor requires large pore sizes to reduce resistance. However, according to the Laplace-Young equation, $\Delta p = 4\sigma\cos\alpha/d_e$ (α is the contact angle), small pores provide large capillary pressure for liquid suction. Vapor release and liquid suction require different pore sizes to achieve better heat performance in LHP. The best approach to solve this problem is to construct multiscale wicks, allowing different behaviors to correspond to different pore sizes. North et al. [17] sintered porous wicks with two pore sizes and reported film evaporation phenomenon in the wicks. The porous wicks satisfied the different requirements for vapor release and liquid suction. The porous wicks prevented the formation of a vapor blanket during the film evaporation process, and thus, the LHP exhibited good heat transfer performance. Semenic and Catton [18] investigated the heat performance of bi-porous wicks and found that thin bi-porous wicks can reach higher critical heat flux (CHF) than monoporous wicks. They showed that bi-porous wicks developed evaporating menisci not only on top surface of the wick but inside as well. The theory of vapor-liquid phase separation was used to explain the findings mentioned above. Yeh et al. [19] prepared bi-porous wicks by controlling the nickel particle diameters, pore former content, and sintering temperature. The results showed there was a clear and strong relationship between the effects of the pore former content and evaporative heat transfer of a bi-porous wick. The evaporative heat transfer coefficient of the bi-porous wick, which can reach a maximum value of 64,000 W/m^2 K, was approximately six times higher than that of the monoporous wick. Lin et al. [20] investigated the heat transfer of LHP with bi-porous and monoporous wicks, through experiments and simulations, and developed a new mathematical model for evaporation heat transfer. The results showed that a bi-disperse wick could decrease the thickness of the vapor blanket region to reach higher heat performance as compared to a monoporous wick. Recently, Li et al. [21] sintered nickel porous wicks and investigated the effects of sintering methods, proportion of pore former, and sintering temperature. Results showed that the optimal wicks sintered at 700 °C, using a cold pressing sintering method, with 30% pore former content by volume. Results also indicated that an LHP with bi-porous wick can start up and run reliably under different heat loads. Although the above studies involved bi-porous wicks, the vapor channel wall was mostly solid. The vapor and liquid can be separated in the vapor channel; however, the separation is not remarkable in the phase change region. To promote vapor-liquid phase separation, sintered porous wicks need to be used to build the vapor channels. Thus, the vapor can enter the channels immediately after evaporation, and porous wicks can supply the liquid sufficiently. Wu et al. [22] and Min et al. [23] validated this mechanism in pool boiling experiments. Ji et al. [24] experimentally found that porous wicks with different pore sizes could effectively separate the flow paths of the vapor and liquid, thereby achieving synergy among different pore sizes. The CHF can reach 3.7 times that on the plain surface.

The start-up of LHP is a complex transient phenomenon, affected by the vapor-liquid phase distribution, structural parameters of wicks, and working conditions. Singh et al. [25] investigated the start-up process of the LHP. At low heat loads, thermal and

hydraulic oscillations were observed. The amplitudes of these fluctuations were very high at condenser inlet and liquid line outlet. The start-up time increases with a decrease in the value of the applied heat load. For very low heat loads, the start-up time was very long and a large temperature difference existed between the evaporator and the condenser. Zhang et al. [26] studied start-up time and temperature oscillation characteristics of the LHP under various conditions. The results showed that the start-up temperature and time increased under anti-gravity operation. However, the opposite phenomenon took place when the vapor channel was filled with liquid. Huang et al. [27] analyzed the start-up of an LHP through experiments and mathematical models. They found that the start-up was closely related to the LHP structure parameters and environment. The start-up phenomena of an LHP can be classified into four modes: failure, oscillating, overshoot, and normal. Recently, Wang et al. [28,29] studied the LHP start-up characteristics. However, a complete regularity of the start-up process has not been obtained due to its complexity. Moreover, Joung et al. [30] found that heat leakage is a key issue concerning LHP heat performance. Large heat leakage can increase the LHP operating temperature and make it difficult to start up.

In this paper, composite multiscale porous wicks were designed and applied to an LHP. This helped solve two contradictory problems. One problem is that the vapor release and liquid flow need large pores to reduce resistance, while the liquid suction requires small pores to provide a large capillary force. The other problem is that the primary layer wick needs high thermal conductivity to improve phase change heat transfer, while the entire wick needs good thermal insulation to reduce heat leakage. Based on this type of composite wicks, the heat transfer and start-up characteristics of the LHP were investigated to explore the optimum structure parameters.

2. Experimental setup and methods

2.1. Experimental setup

Experimental setup consists of a test section (LHP), a power control system, heating components, and a data acquisition system. The LHP is placed on a rotating platform to adjust the angle between the heat pipe and the horizontal plane. The details are as follows:

(1) Fig. 1(a) shows the whole structure of an LHP and Table 1 shows the corresponding structure parameters. The LHP is mainly made up of copper and has planar sizes of 300.0 mm × 300.0, 400.0, and 500.0 mm. In the operation process, the liquid in the LHP needs to overcome resistance and go through a distance from the condenser to evaporator. This distance is called the liquid line length (L_l). Here, there are three liquid line lengths, L_l = 300.0, 400.0, and 500.0 mm. In Fig. 1(a), the LHP consists of five parts: an evaporator, compensation chamber, vapor line, liquid line, and condenser. To study the effects of various parameters, different structure evaporators were made (see Fig. 2 and Table 2 for details). The commercial condenser has a planar size of 130.0 mm by 130.0 mm with a thickness of 25.0 mm, and includes 53 aluminum fins. Each fin has a thickness of 0.2 mm. A 5 W fan was used to cool the condenser under room temperature. Both the liquid and vapor lines have an outer diameter of 8.0 mm and inner diameter of 6.0 mm. The location and distribution of the temperature measuring points are also shown in Fig. 1(a). Starting from the vapor outlet, the thermocouples are marked as T_{Eout}, T_V, T_{Cin}, T_{C1}–T_{C4}, T_{Cout}, T_{CPin}, and T_{CP}. T_{Eout} measures the vapor temperature at the vapor outlet port, where a thermocouple is inserted into the vapor line. T_V measures the outer wall temperature of the vapor line. T_{Cin} and T_{Cout} measure the tube temperature of the condenser

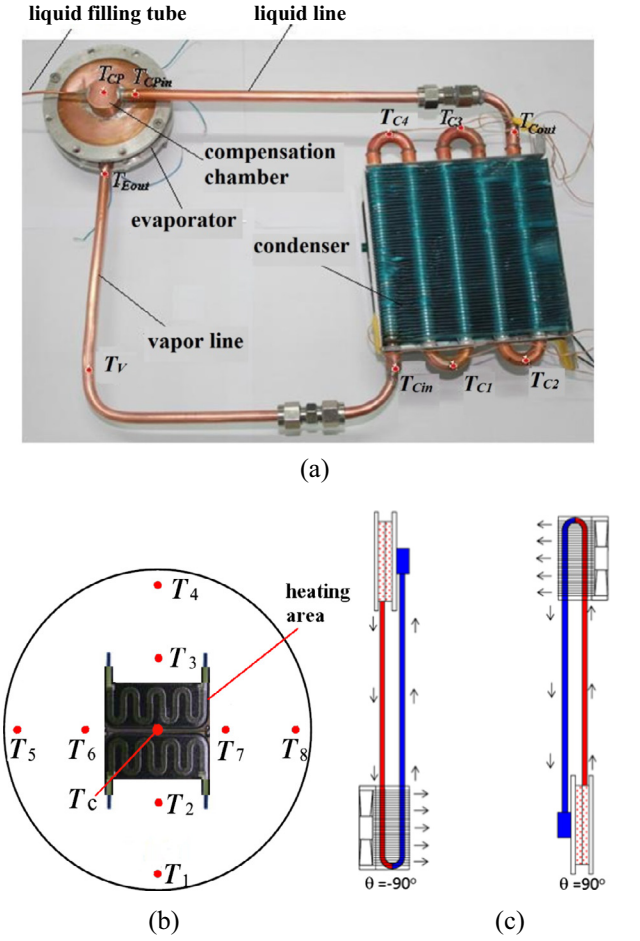

Fig. 1. Experimental setup: (a) loop heat pipe; (b) distribution of temperature measuring points on the evaporator bottom wall; and (c) schematic diagram of tilt angles for loop heat pipe.

Table 1
Structure parameters of loop heat pipe.

Porous material	Copper powder and absorbent wool
LHP material	Copper
Planar LHP size	300.0 mm × 300.0, 400.0 and 500.0 mm
Evaporator outer diameter	D_e = 80.0 mm
Evaporator thickness	10.0 mm
Evaporator inner diameter	72.0 mm
Evaporator wall thickness	1.0 mm
The primary layer wick	
Thickness	2.0 mm
Diameter	D_{ei} = 68.0 mm
Copper powder particle size	Four particle species are used
The second layer wick	
Thickness	2.0 mm
Diameter	D_{ei} = 68.0 mm
Copper powder particle size	Average diameter d_p = 149 μm
The third layer wick	
Thickness	2.0 mm
Diameter	D_{ei} = 68.0 mm
Vapor line length	550.0, 650.0 mm and 750.0 mm
Inner/outer diameters of vapor and liquid tube	6.0 mm/8.0 mm
Condenser size	130.0 mm × 130.0 mm × 25.0 mm
Liquid line length	L_l = 300.0, 400.0 and 500.0 mm
Heating area	5.0 cm^2 or 25.0 cm^2

at the inlet and outlet ports, respectively. T_{C1}–T_{C4} measure the tube wall temperatures on the four tube bending sections. T_{CPin} measures the wall temperature of the liquid line near the compensa-

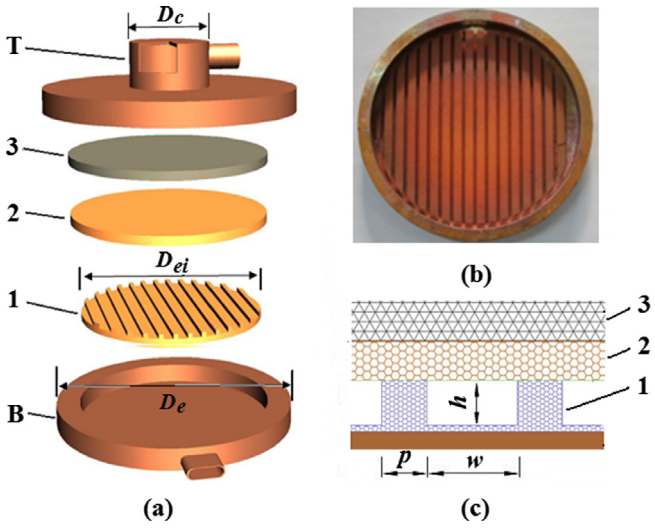

Fig. 2. (a) Split structure of the evaporator, wicks, and compensation chamber (*T*: top cover, *B*: bottom cover, 1: primary layer wick, 2: second layer wick, 3: third layer wick); (b) the primary layer wick sintered on the evaporator bottom wall; and (c) the position relation of three layer wicks.

tion chamber. T_{CP} measures the liquid temperature inside the compensation chamber. Two thin film heaters, with a snake like shape and which were attached on the bottom evaporator surface using a silver silica gel, to fill the gap between the film heater and evaporator surface, were used to heat the evaporator (see Fig. 1(b)). The heaters have heating areas of 5.0 and 25.0 cm^2, respectively, and are surrounded by heat insulation materials to reduce heat loss. Nine thermocouples were welded on the evaporator surface; where T_C measures the temperature of the evaporator center wall and T_1–T_8 measure other location temperatures on the evaporator wall to investigate the temperature distribution. Tilt angle $\theta = -90°$ or 90° refers to the evaporator above or below the condenser (see Fig. 1(c)), and $\theta = 0°$ refers to the condenser and evaporator being in the same horizontal level. At $\theta = -90°$, the liquid has to overcome gravity to flow. Thus, L_l is also called anti-gravity height.

(2) The power control system is made up of a 220 V power supply, a voltage regulator, and a power-meter. The voltage can be adjusted from 0 to 220 V by the voltage regulator. Thus, the power control system can supply power from 0 to 500 W and the maximum heat flux is 90 W/cm^2. The heat power can be read from the power-meter. A Hewlett-Packard data acquisition instrument was applied to collect all the data.

(3) Fig. 2(a) shows the split structure of the evaporator, wicks, and compensation chamber. The evaporator has a diameter of 80.0 mm and a thickness of 10.0 mm (excluding the compensation chamber height), and consists of a top cover (*T*), bottom cover (*B*), and porous wicks with three layers (1–3). The compensation chamber is integrated with the top cover, which is necessary for the liquid supply and start-up of the LHP. For conventional LHP, the groove wall in the evaporator is solid. However, in our LHP, it was replaced by sintered porous wick, called primary layer wick. Fig. 2(b) shows the primary porous wick sintered on the bottom wall of the evaporator. Parallel and circular grooves were formed by sintering to provide vapor paths. Fig. 2(c) shows the position relation of the three layer wicks, where the groove depth, width, and groove wall width are marked as *h*, *w*, and *p*, respectively. To decrease the flow resistance of the liquid, the copper powder with large particle diameter (d_p = 149 μm) was used to sinter the second layer wick. The third layer wick was made of absorbent wool with good liquid absorption and thermal insulation. Thus, three layer wicks formed a composite wick.

(4) Table 2 shows 11 kinds of LHPs. Their difference is reflected mainly in the structure parameters of the primary layer wick. They can be divided into three types: (1) Solid groove LHP (#1). The groove wall is solid, which is common in conventional LHPs. (2) Uniform porous groove LHP (#2–149, 149 stands for d_p = 149 μm). The groove wall is fabricated by sintering copper powder with large particle diameters. The particles cannot form clusters in the sintering process. (3) Bi-porous groove LHP (#2–13, #2–37, #2–88, and #3–8). The groove wall is also formed by sintering, however small particles can form clusters in the sintering process. These grooves have depths of 1.0, 1.5, and 2.0 mm, widths of 1.0, 1.5, and 2.0 mm, and groove wall widths of 2.0, 3.0, and 4.0 mm, respectively. Four kinds of copper powder, with average particle diameters of 149, 88, 37, and 13 μm, were used to sinter porous wicks. For all the LHPs, the second layer wick, with average particle diameter of 149 μm, directly covers the grooves.

(5) Fig. 3 presents the scanning electron microscopy (SEM) images of the primary layer wick. In Fig. 3(a), the image is showed as side view, which is sintered with d_p = 149 μm. Fig. 3(b) shows the image as top view (d_p = 88 μm). In the wicks, the grooves are for the vapor to go out and the porous groove walls are for the liquid to be sucked in. Fig. 3(c)–(f) shows the microstructures of wicks with different particle diameters. In Fig. 3(c), the particles are large and spherical with a diameter of 149 μm. After Fig. 3(c), the diam-

Table 2
Types of loop heat pipe and primary structures adjacent to the evaporator wall.

LHP	Primary structures adjacent to the evaporator wall	Groove depth *h* (mm)	Groove wall width *p* (mm)	Groove width *w* (mm)	Groove types and particle sizes (μm)
#1	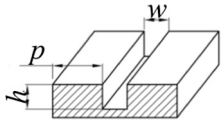	1.5	3.0	1.5	Solid groove wall
#2–13	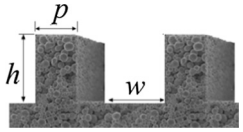	1.5	3.0	1.5	Bi-porous groove wall, d_p = 13 μm
#2–37					Bi-porous groove wall, d_p = 37 μm
#2–88					Bi-porous groove wall, d_p = 88 μm,
#2–149					Uniform porous groove wall, d_p = 149 μm
#3		1.5	4.0	1.5	Bi-porous groove wall, d_p = 88 μm
#4		1.5	2.0	1.5	
#5		1.5	3.0	1.0	
#6		1.5	3.0	2.0	
#7		1.0	3.0	1.5	
#8		2.0	3.0	1.5	

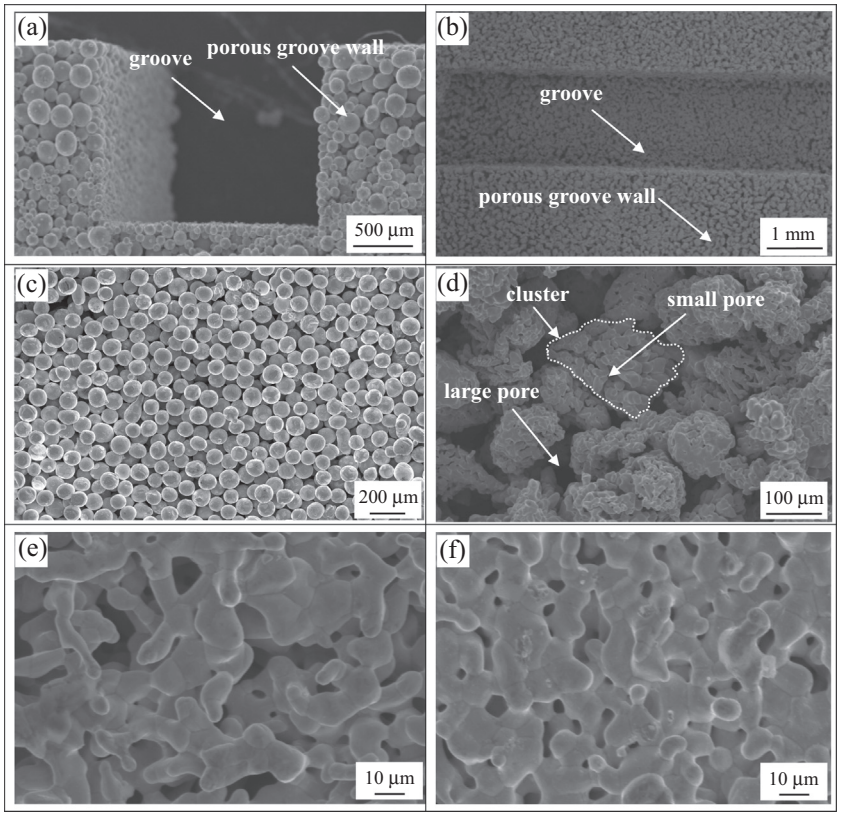

Fig. 3. SEM images for primary layer wicks: (a) side view; (b) top view; (c) for d_p = 149 μm; (d) for d_p = 88 μm; (e) for d_p = 37 μm; and (f) for d_p = 13 μm.

eters of the particles decrease gradually and they bond with each other, forming clusters, especially for wicks with a particle diameter of 88 μm (see Fig. 3(d)). As seen in Fig. 3(d), small pores exist in the clusters and large pores exist among clusters. A large pore is about ten times the size of a small pore. When large and small pores are coupled with a groove, the primary layer wick forms multiscale structure, with nano, micro, and millimeter scales. Fig. 3(e) and (f) shows the images of wicks for d_p = 37 μm and 13 μm. It is obvious that small diameter particles easily form clusters in the sintering process; however, the amounts of the large and small pores decrease. The significant difference between our design and the conventional one is shown in Fig. 4. For conventional design (see Fig. 4(a)), grooves are machined on the evaporator substrate. There is a monoporous layer wick above the grooves, which functions as a place for the liquid supply and evaporation. There are three disadvantages: (1) the evaporation area is small due to the solid groove wall; (2) at high heat fluxes, a vapor blanket layer is formed easily within the wick, which raises thermal resistance and deteriorates heat transfer; (3) the vapor gets easily into the compensation chamber. Thus, the LHP has a large heat leakage, which hinders the circulation of the working fluid and worsens the heat performance of the LHP, or causes the LHP to stop working. However, an LHP with composite multiscale porous wicks has the following advantages (see Fig. 4(b)): (1) The vapor channels are constructed by porous wicks, hence the evaporation area is large. (2) The primary layer wick separates the flow paths of the vapor and liquid, and resolves the conflict between vapor release and liquid suction (large pores for vapor venting and small pores for liquid suction). (3) The second monoporous wick and third layer wick function not only as paths for liquid supply, but also as thermal barriers, which reduce heat leakage from evaporator to compensation chamber. There are two reasons for having thermal barriers: on one hand, the third wick layer has an ultra-low thermal conductivity, and on the other hand, when the second layer wick is filled with water, it will prevent vapor from entering the compensation chamber.

2.2. Experimental processes and methods

The most important part of these experiments is to prepare porous wicks. Before sintering, the evaporator bottom cover was first cleaned using methanol and distilled water, to ensure that the working fluid wetted the porous wicks and evaporator wall, and avoided contaminants producing non-condensable gas. Then, the evaporator bottom cover was baked in an oven, next copper powder was spread on the graphite mold, and evaporator bottom cover was pressed onto it with a certain pressure. Finally, they were all put into the furnace to sinter the primary layer wick. The furnace was vacuumed and then charged with a mixture of hydrogen and nitrogen gases to prevent wick oxidation. The maximum sintering temperature was set at 950 °C. A four-step sintering procedure was used. After the primary layer wick was sintered and removed from the furnace, the grooves of the primary layer wick were filled with sodium chloride (NaCl) particles. The copper powders were spread on the primary layer wick. Then, a ceramic plate was used to press on the copper powders, and the next sintering process was the same as that of the primary layer wick. Hence, the second layer wick was sintered on the primary layer wick and two layer wicks were combined together. After putting absorbent wool on the second layer wick, a complete composite multiscale wick with three layers was obtained. After completing the LHP assembly, a bubble method was employed to check its sealing performance, i.e., the LHP was charged with an air pressure of 0.3 MPa and put in hot water at 50 °C. If no bubbles were generated, it meant that the LHP was packaged well and available for experiments.

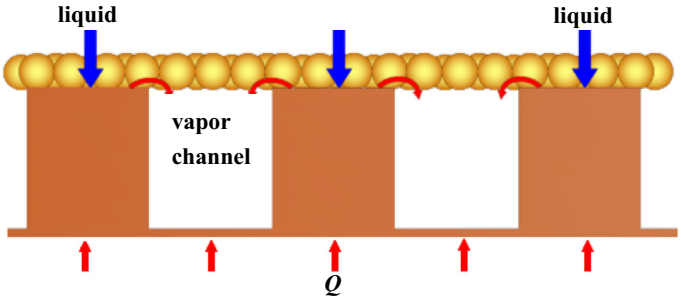

(a) Conventional wick structure

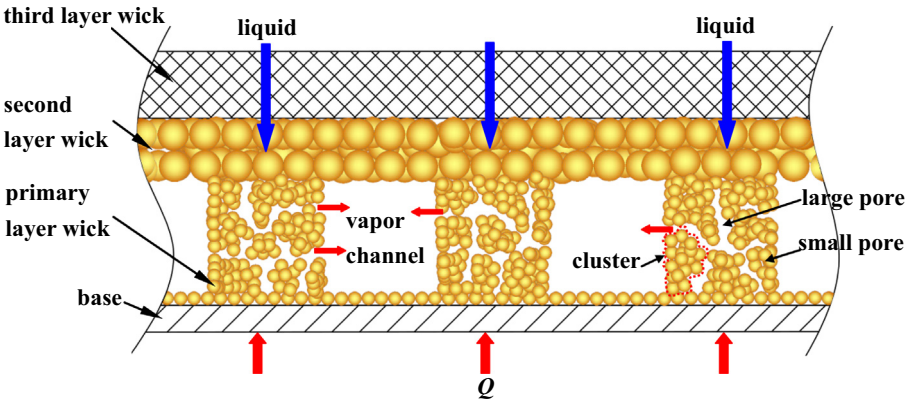

(b) Composite wick structure

Fig. 4. Structure of a wick: (a) conventional structure; (b) composite wick structure.

To reduce the effect of non-condensable gas as much as possible, a little distilled water was first injected into the LHP to get rid of non-condensable gas stored in the pores of wicks, as it is difficult to eliminate. Then the LHP was heated and vacuumed simultaneously, keeping the evaporator bottom center temperature between 50 °C and 100 °C. When the pressure reached 0.06 Pa, a certain amount of distilled water was charged into the LHP. The liquid filling ratios (ϕ), which is defined as the liquid volume divided by the total LHP volume, was 38.5%, 51.3%, and 64.1%. Each experiment was started at a low heat load. The interval was 10 or 20 W until the heat load exceeded the limit of the heat pipe or heater power.

2.3. Data reduction

Film heaters are wrapped by thermal insulation materials except the side on which the heat is exchanged with the evaporator bottom wall. Now, the heat flux on the evaporator wall can be expressed as:

$$q = \frac{Q}{A} \tag{2}$$

where Q is the heat load, and A is the heating area. The evaporator, LHP, and total thermal resistances can be expressed respectively as:

$$R_e = (T_C - T_{Eout})/Q \tag{3}$$

$$R_L = \left(T_C - \frac{T_{Cin} + T_{Cout}}{2}\right) \Big/ Q \tag{4}$$

$$R_t = (T_C - T_{air})/Q \tag{5}$$

where T_{air} is the ambient temperature. In the present experiments, the temperature measurement has a maximum uncertainty of 0.3 °C, and the heat load and geometry size measurement have a relative error of 0.5% and 1%, respectively. Thus, the uncertainty of the thermal resistance is 4.3%.

When the evaporator is heated, the heat is divided into two parts: one part changes liquid into vapor (Q_{vap}); and the other part is delivered to the liquid in the compensation chamber as heat leakage (Q_{CP}), which can be expressed as:

$$Q_{CP} = m_f c_p (T_{CP} - T_{Cout}) \tag{6}$$

$$m_f = Q_{vap}/r \tag{7}$$

where m_f is the mass flow rate, c_p is the specific heat capacity, and r is the latent heat of vaporization. Due to $Q = Q_{CP} + Q_{vap}$, the heat leakage percentage can be expressed as:

$$\beta = \frac{Q_{CP}}{Q} = \frac{(T_{CP} - T_{Eout})}{(T_{CP} - T_{Cout}) + r/c_p} \tag{8}$$

Through calculation, the heat leakage is found to have an uncertainty of 6.4%.

3. Results and discussion

3.1. Start-up of LHP

The LHP start-up refers to the process in which the evaporator is heated to a steady state. It can be divided into two stages: stage I and II (see Fig. 5(a)). At stage I, the evaporator begins to be heated and T_C begins to rise. However, T_{Cin} does not rise. The time for this stage is defined as t_1. The stage II refers to the process from the sharp rise of T_{Cin} to the LHP reaching the steady state. The rise of T_{Cin} means that the vapor has reached the condenser. The time taken for this stage is defined as t_2 and the start-up time is defined as $t = t_1 + t_2$. Fig. 5 shows the start-up processes of solid groove LHP (#1 in Table 2) and bi-porous groove LHP (#2–88 in Table 2) at

L_l = 300.0 mm, θ = 90°, and Q = 20 W. During the start-up processes, T_{Cout} remains constant. T_{CP} remains unchanged at the beginning and rises slightly later. T_C has the quickest response, because it is near the heaters and T_{Cin} responds slowly as it is far away from the heaters. From Fig. 5(a)–(c) and (d)–(f), the time spent in stage I is longer than that in stage II both for #1 and #2–88. Moreover, the start-up time and T_C both increase with an increase in the liquid filling ratio. However, the heat performance of #2–88 is better than that of #1 under three liquid filling ratios. For example, under the same conditions (see Fig. 5(b) and (e), ϕ = 51.3%), #2–88 has T_C of 43.3 °C and start-up time of 159 s, while #1 has T_C of 51.5 °C and start-up time of 338 s. The start-up temperature of #2–88 is reduced by nearly 8 °C, and start-up time is reduced by 179 s. Besides, Fig. 5(e) shows that #1 has an obvious temperature oscillation. However, the temperatures are stable for #2–88 under most conditions. In summary, the composite multi-scale porous wicks

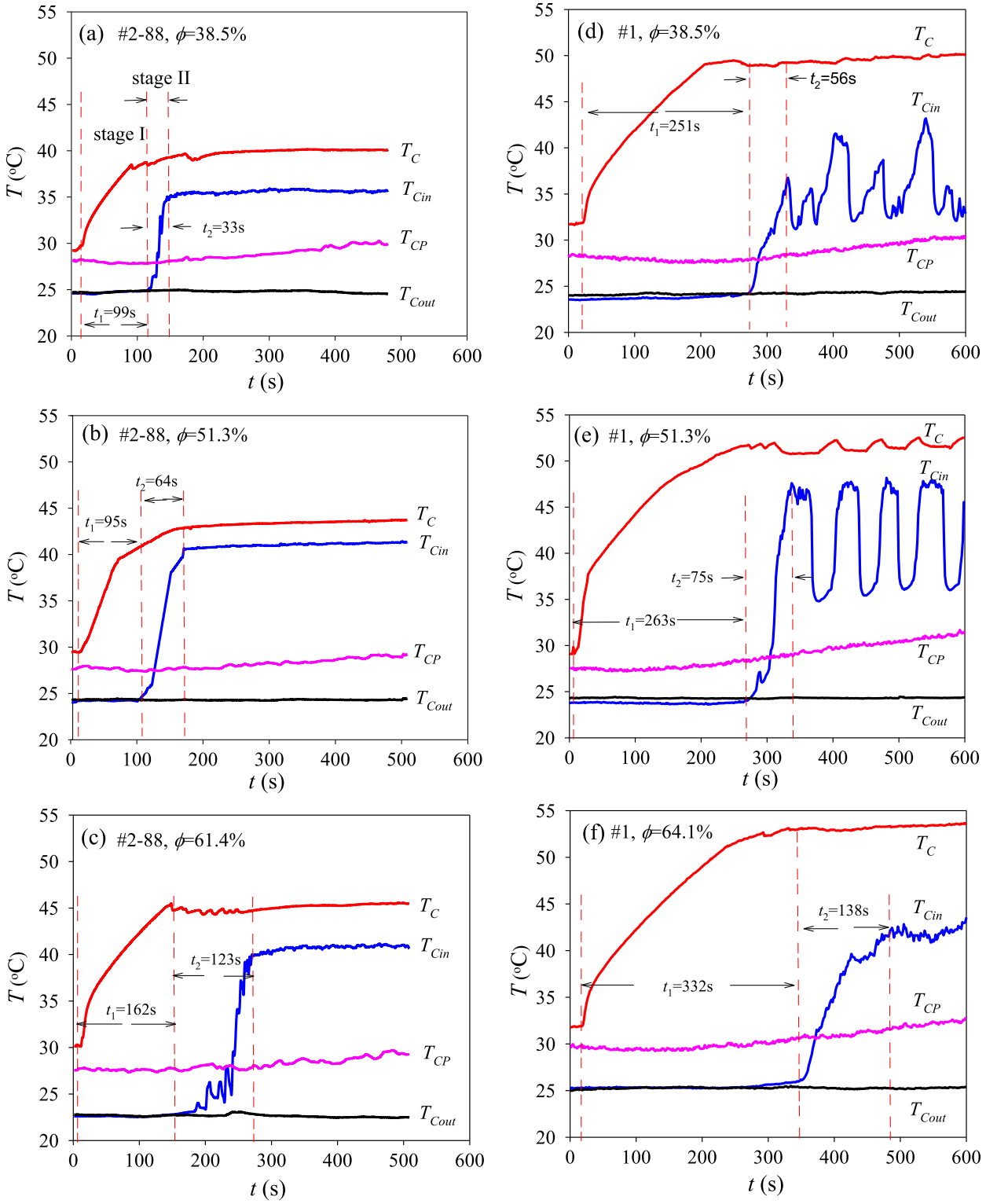

Fig. 5. Start-up of loop heat pipe under different filling ratios: (a), (b), and (c) for #2–88; (d), (e), and (f) for #1 (L_l = 300.0 mm, Q = 20 W, θ = 90°).

significantly shorten the start-up time, decrease the evaporator wall temperature, and suppress the temperature instability during the start-up process. Because different from conventional LHPs, our LHP does not contain solid groove micro-channel. In fact, it directly receives heat from the heater to initiate the phase change heat transfer within porous wicks. Thus, our LHP not only has a short start-up time, but also a low wall superheat to avoid the phenomenon of boiling hysteresis. Besides, as per the traditional view [25], temperature oscillations of the whole system are expected to be the outcome of the heat leak fluctuations from the evaporator to the compensation chamber and subcooled liquid from the condenser. Due to good thermal insulation of the composite wicks, our LHP has low heat leakage from evaporator to compensation chamber and the corresponding temperature oscillation is suppressed.

For LHP, the tilt angle $\theta = 90°$ is the most common working environment. At $\theta = -90°$ and $\theta = 0°$, the start-up processes of #1 and #2–88 are shown in Fig. 6. Compared with #1, #2–88 shows better start-up performances, having shorter start-up time and lower evaporator wall temperature. The regulation is similar to that at $\theta = 90°$. The effects of the tilt angles are discussed in the latter section.

Fig. 7(a) shows the start-up process for #2–88 at low heat load ($L_l = 300.0$ mm, $\phi = 51.3\%$, $\theta = 0°$). At $Q = 10$ W, if the LHP cannot start up for some reason, T_C will reach a certain temperature and then become stable. However, the sharp rise of T_{Cin} does not take place and T_{CP}, too, remains at low temperature. In such situation, if the heat load continues to increase rapidly to 20 W on the basis of 10 W, the LHP will start up. However, T_C and T_{Cin} are larger than those for directly heating from a 20 W heat load, which indicates that it is harmful if the LHP cannot start up at a certain heat load. The greater the heat load, the greater the harm. However, in present experiments, the failed start-up process did not take place at high heat load. Fig. 7(b) shows the start-up process at high heat load $Q = 170$ W. High heat load shortens the start-up time for all LHPs, especially for #2–88. #2–88 only takes about 50 s to start up, while #1 takes about 150 s. After start-up, the T_C of #2–88 at three tilt angles is lower than #1, and the maximum difference goes up to 25 °C. Under the anti-gravity situation ($\theta = -90°$), #2–88 has the quickest start-up and lowest T_C among the three tilt angles.

To investigate the start-up characteristics of an LHP with composite multi-scale porous wicks, the effects of various factors were studied. The findings are as follows:

(1) Effects of liquid filling ratios and tilt angles

Fig. 8(a) shows the effects of liquid filling ratios on the start-up time for #1 and #2–88 at $Q = 20$ W. Overall, smaller liquid filling ratio yields shorter start-up time. However, it is not obvious when the liquid filling ratio is less than 51.3%, and when it is beyond 51.3%, the start-up time increases with an increase in the filling ratios. The increase in t_1 is the main reason for the increase in the total start-up time. The accumulation of liquid in the evapora-

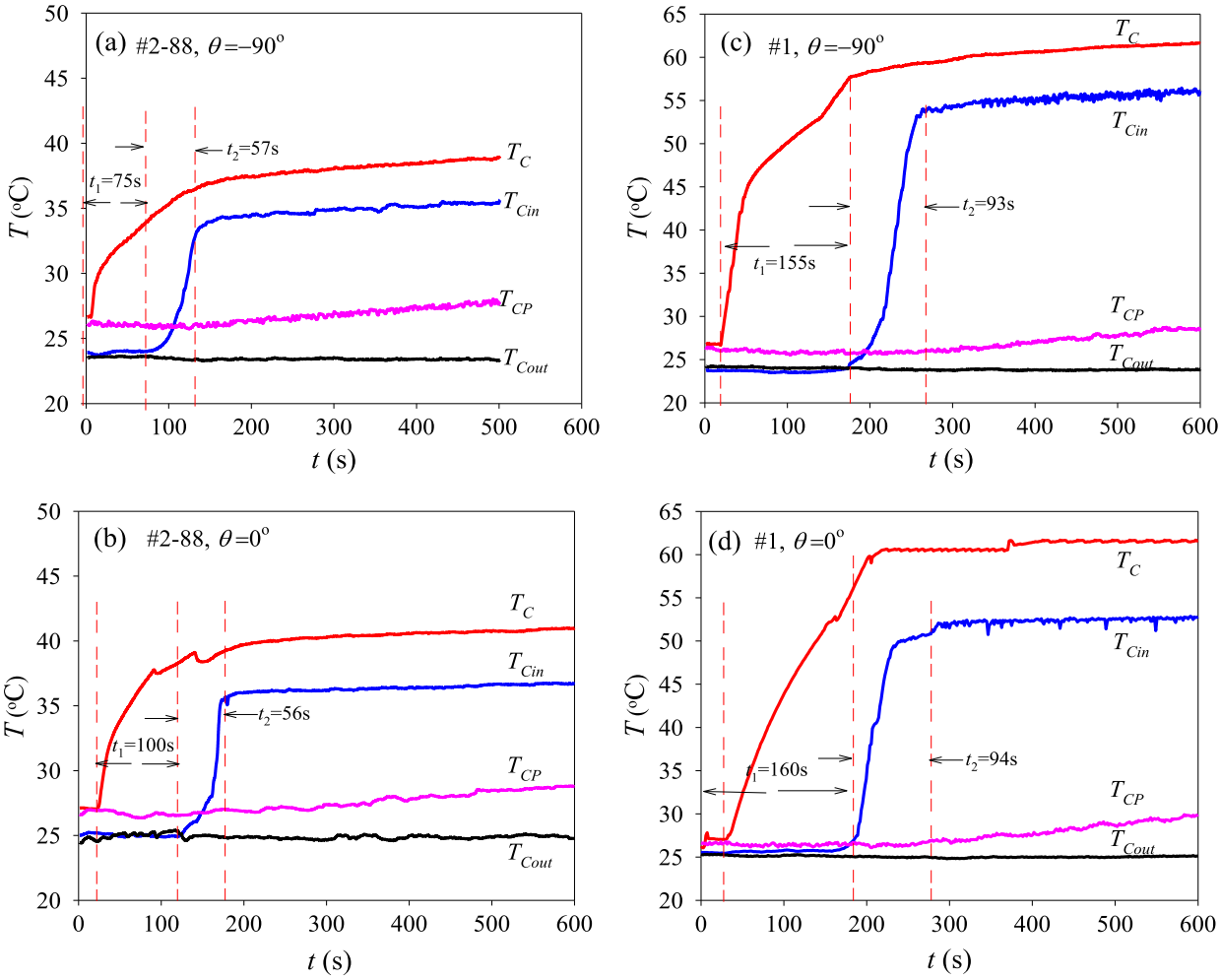

Fig. 6. Start-up of loop heat pipe under different tilt angles: (a) and (b) for #2–88; (c) and (d) for #1 ($L_l = 300.0$ mm, $Q = 20$ W, $\phi = 51.3\%$).

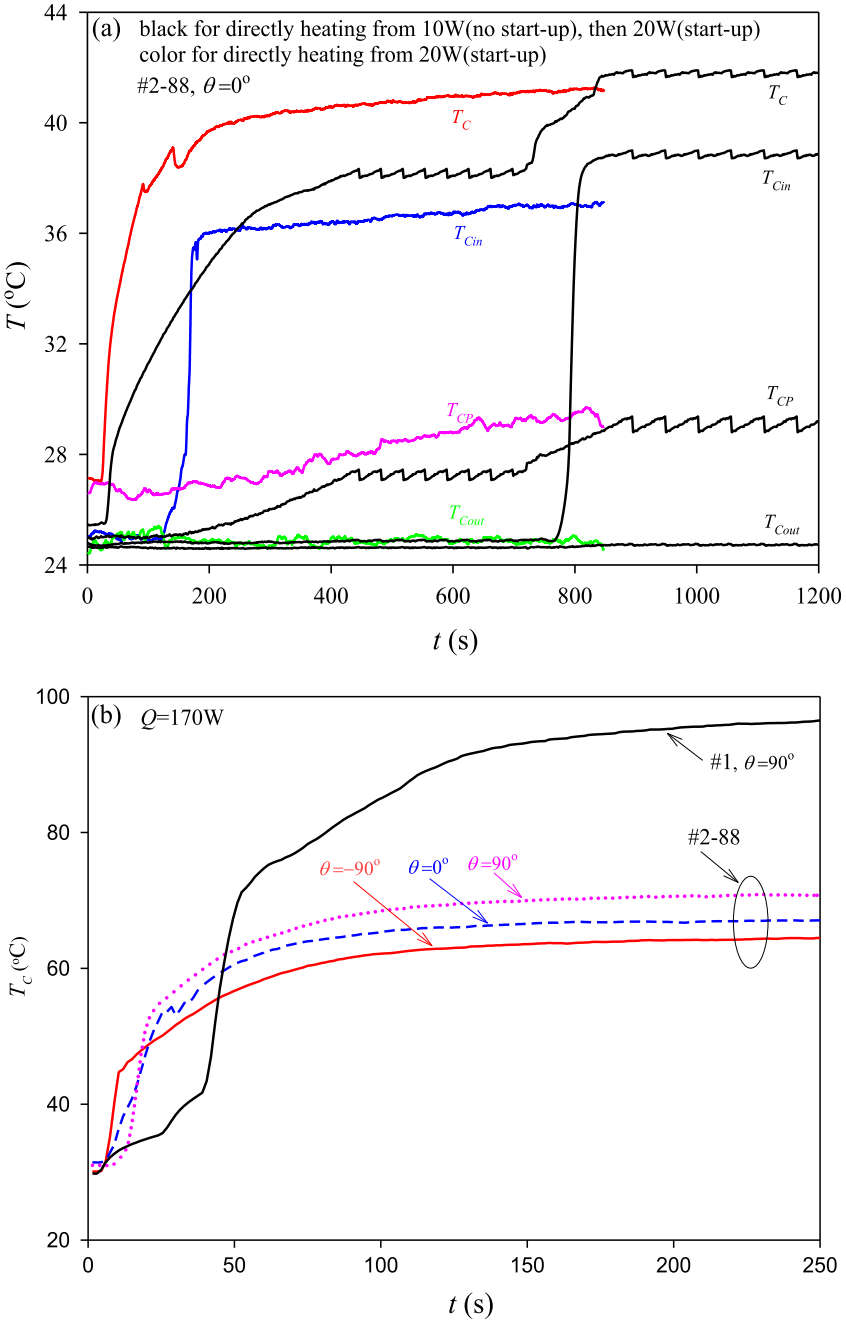

Fig. 7. Start-up of loop heat pipe at low and high heat load: (a) for $Q = 10$, 20 W; (b) for $Q = 170$ W ($L_l = 300.0$ mm, $\phi = 51.3\%$).

tor increases with an increase in the filling ratios. Too much liquid can block the vapor release when the evaporator bottom cover reaches a certain superheat. Compared with #1, the start-up time of #2–88 was reduced by 53%. Fig. 8(b) shows the effects of tilt angles on the start-up time for #2–88 at $\phi = 51.3\%$. The start-up time becomes longer with the increase in the tilt angles. The shortest start-up time of 121 s appears at $\theta = -90°$. Under the anti-gravity operation, the vapor is less hindered by the liquid accumulated in the evaporator.

(2) Effects of primary wick structure

The effects of wick structure parameters on the start-up time can be seen in Fig. 9 ($L_l = 300.0$ mm, $\phi = 51.3\%$, $Q = 20$ W, $\theta = -90°$), relating to #2–88 and #3–8. When the groove wall width and depth are kept constant, the start-up time varies with the groove width (see Fig. 9(a)). The start-up process takes a long time when the groove width is small, because a small channel hinders the vapor from venting. When w is less than 1.5 mm, the start-up time decreases with an increase in the groove width. When w is more than 1.5 mm, the start-up time increases with an increase in the groove width, because the vapor mass and volume are small at low heat load. Thus, if the groove is too wide, the pressure of vapor is not sufficient to push them into the condenser. There is an optimal groove width of 1.5 mm in present experiments. Fig. 9(b) shows that the start-up time varies with the groove depth. The start-up time decreases with an increase in the groove depth at $h < 1.5$ mm. If the groove depth is too small, the start-up time is long, because the vapor encounters a large resistance while leaving the channel. However, the start-up time increases with the increase in the groove depth at $h > 1.5$ mm. If the groove is too deep, the path length of heat transfer increases, which is not

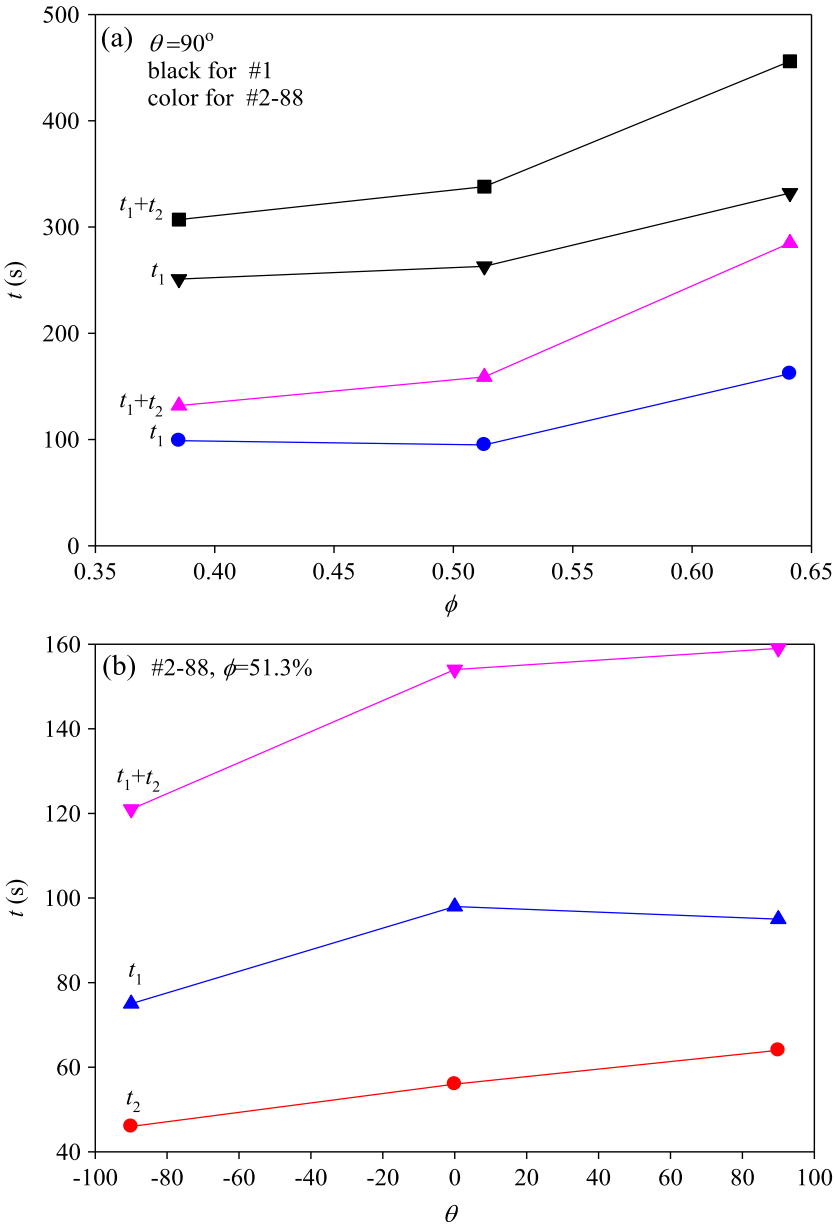

Fig. 8. Effects of filling ratios (a) and tilt angles (b) on the start-up time (L_l = 300.0 mm, Q = 20 W).

beneficial for liquid vaporization as it decreases the pressure of vapor at low heat load. The shortest start-up time appears at h = 1.5 mm among the three depths. Fig. 9(c) shows the effect of the groove wall width. The start-up time decreases with the increase in the groove wall width at p < 3.0 mm. When the groove wall is narrow, the start-up time is long due to the small evaporation area and small liquid supply. However, the start-up time has little change at p > 3.0 mm. Because both the evaporation area and resistance of vapor release increase with the increase in the groove wall width, there is a balanced relationship between them after the evaporation area reaches a certain value. In summary, for #2–88, the optimal groove width, groove depth, and groove wall width are w = 1.5 mm, h = 1.5 mm, and p = 3.0 mm, respectively.

(3) Effects of particle diameters and liquid line lengths

Fig. 10(a) shows the effects of particle diameters on the start-up time for #2–13, #2–37, #2–88, and #2–149. In general, a smaller particle diameter leads to longer start-up time. The reason is that if the particle diameters are too small, the gaps among the particles decrease. Hence, the resistance of vapor venting becomes large. As indicated by the tendency, the start-up time is shortened with the increase in the particle diameters at d_p < 40 μm; however, the start-up time undergoes little change at d_p > 40 μm. The shortest start-up time appears at d_p = 88 μm in our test. Fig. 10(b) shows that for #2–88, the start-up time increases with the increase in the liquid line lengths at θ = 0° and Q = 20 W. At low heat load, the length has little effects on t_1. The increase of t_2 is the main reason for the increase of the total start-up time. As the length increases, the vapor will take longer time to travel from evaporator to condenser.

3.2. Thermal performances

3.2.1. Transient temperature

Fig. 11(a) shows T_C versus time at θ = 0° and θ = 90°. For both #1 and #2–88, T_C increases with the increase in the heat load. At low or moderate heat load, for the same LHP, T_C almost has a parallel

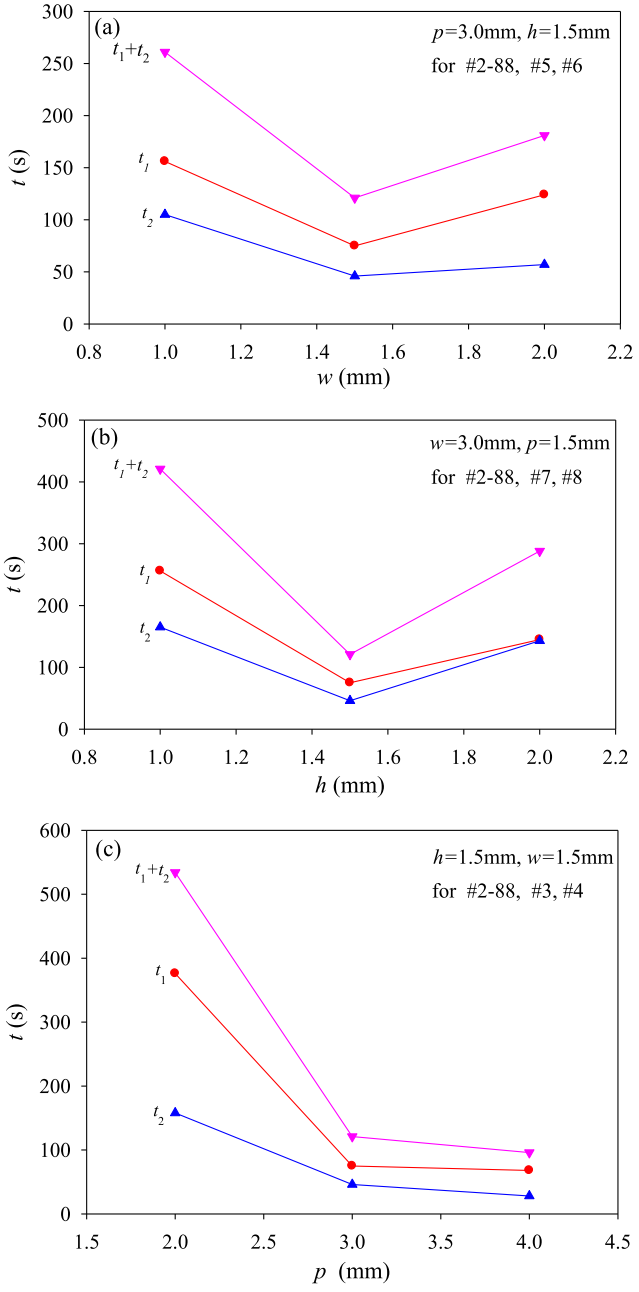

Fig. 9. Effects of wick structure parameters on the start-up time: (a) for different w; (b) for different h; (c) for different p (L_l = 300.0 mm, ϕ = 51.3%, Q = 20 W, θ = −90°).

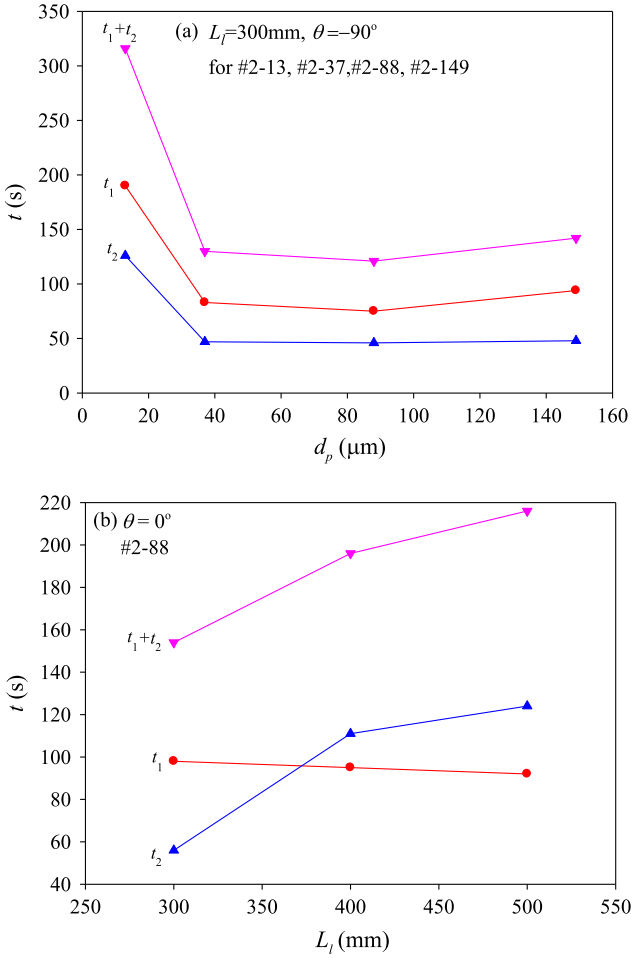

Fig. 10. Effects of particle diameters (a) and liquid line lengths (b) on the start-up time (Q = 20 W, ϕ = 51.3%).

development with increasing heat loads at θ = 0° and θ = 90°, and at high heat load, the T_C values tend to be close to each other. It means that the effects of structure parameters and tilt angels on the thermal performance of LHP have already been manifested during the start-up process. Because, it is difficult to start up for #1 at Q = 10 W, a 20 W heat load was given directly to start it up. After being started up at Q = 20 W, T_C is 62.5 °C and 51.3 °C at θ = 90° and θ = 0°, respectively. The gravity auxiliary condition is beneficial for LHP operation at Q < 120 W; however, the heat performance of the LHP begins to deteriorate and T_C increases rapidly at Q > 120 W. Only at Q = 180 W, T_C reaches 97 °C at θ = 90°. However, for #2–88, it can be started up at 10 W, at which T_C is only about 40 °C. Even when the power is up to 200 W, T_C is only 70 °C. Compared with #1, T_C of #2–88 is reduced by 30 °C at Q = 160 W and θ = 90°. Attention was paid to the anti-gravity characteristics of #2–88 (see Fig. 11(b)). The LHP can be started up at Q = 10 W and θ = −90°, T_C is only 36 °C, indicating the start-up temperature is quite low. After start-up, T_C increases with increasing heat loads. When the heat load increases by 10 W, the temperature rises by about 2–3 °C (except the start-up process). T_C reaches 63 °C at Q = 200 W, which is lower by 7 °C approximately than that at θ = 0°. T_C is 56 °C at Q = 160 W, which is lower by 41 °C approximately than that of #1 for the same tilt angle. Hence, compared with #1, #2–88 has an excellent anti-gravity ability and better heat performance under the anti-gravity condition. To understand the operating characteristics of this excellent loop heat pipe, Fig. 11 (b) also shows the transient change of T_{Cout}, T_{CP}, and T_{Cin}. In the whole process, T_{Cout} is kept at room temperature. T_{Cin} has a large rise during the start-up process, and then increases gradually with increasing heat loads. T_{CP} slightly increases with increasing heat loads at Q < 80 W, and then decreases with LHP operation at high heat load. Finally, it begins to rise again due to the large heat leakage.

3.2.2. Resistance analysis

There are many factors affecting the heat transfer of LHP, including liquid filling ratios, structure parameters of wicks, tilt angles, heating area, and heat load. Porous copper wicks used in present experiments have high thermal conductivity, which enhances the solid-liquid effective thermal conductivity to improve phase change heat transfer. Moreover, the wicks have

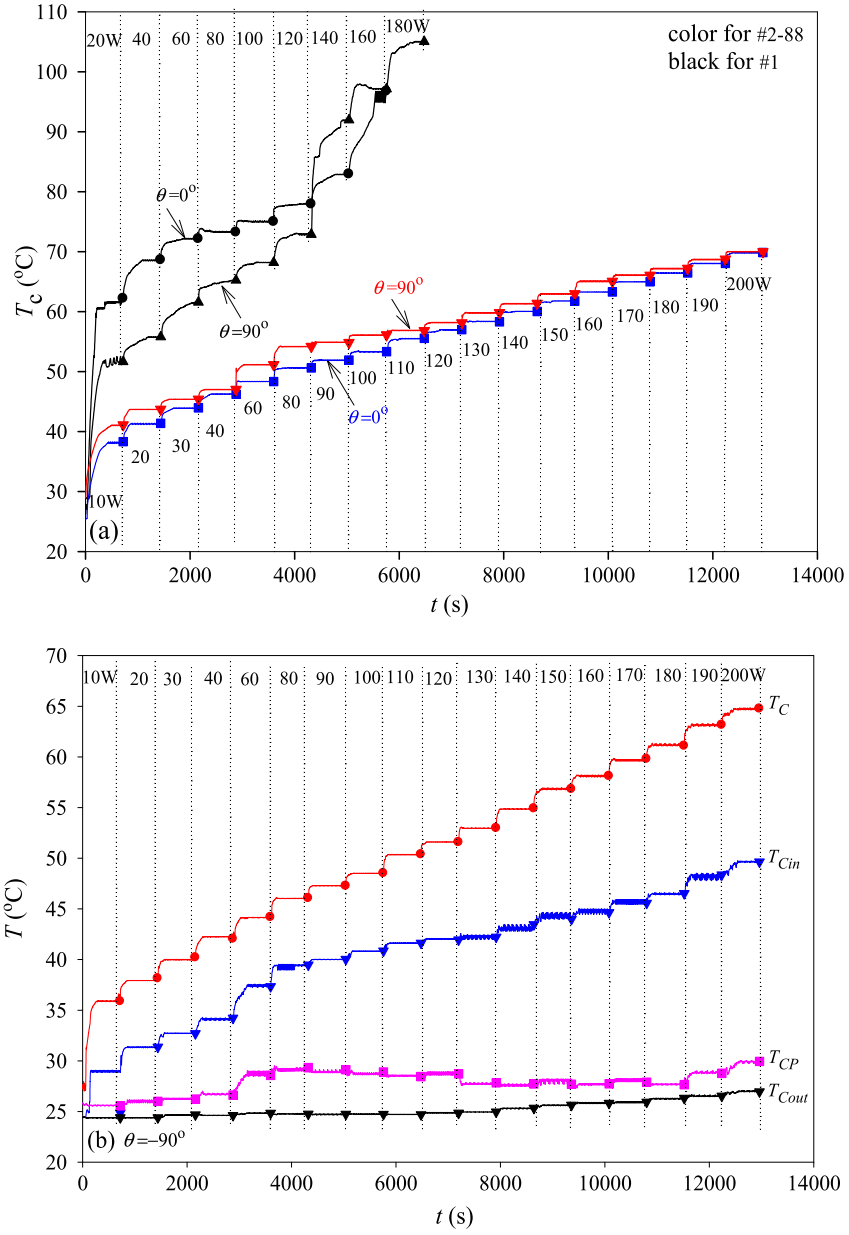

Fig. 11. Transient temperature versus time: (a) comparison of center temperature between #1 and #2–88; (b) temperature of different measuring points at $\theta = -90°$ for #2–88 (L_l = 300.0 mm, ϕ = 51.3%).

multi-scale structure with large pores and small pores. Large pores reduce the resistance of vapor release and small pores produce great capillary pressure acting as driving force for liquid circulation. Some analyses have been reported in previous literatures. Here, only the effects of heating area and liquid line length of the LHP on the thermal resistance are discussed.

(1) Effects of heating area

Fig. 12 shows the effects of the heating area on the total thermal resistance, evaporation thermal resistance, and LHP thermal resistance. For #2–88, there are two heating areas of 25 cm^2 and 5 cm^2. The thermal resistance of a large heating area is larger than that of a small area at low heat load. However, the thermal resistance is less affected by the heating area at high heat load. The most obvious effects of the heating area on the thermal resistance appear at $\theta = -90°$ and 90°. There are two distinct regions to be divided. They are the nucleation boiling region and liquid film evaporation region (see Fig. 12(a)). The transition point is about Q = 100 W at θ = 90°. At low heat load (Q < 100 W), the LHP operates in the nucleation boiling region. A large heating area, corresponding to low heat flux, causes few nucleation sites and hence, the evaporator thermal resistance is large. However, when the LHP operates in the film evaporation region, the number of nucleation sites has a smaller effect on the heat transfer. Thus, the thermal resistance is less affected by heat flux and more affected by heat load. Compared with the situation at θ = 90°, the heat load range of the nucleation boiling region extends at $\theta = -90°$ (see Fig. 12(b)). The transition point appears at Q = 170 W. Because there is little liquid accumulation in the evaporator at $\theta = -90°$, the vapor goes out of evaporator with a small resistance under a low saturated vapor pressure. This is why the LHP has a small thermal resistance and excellent heat

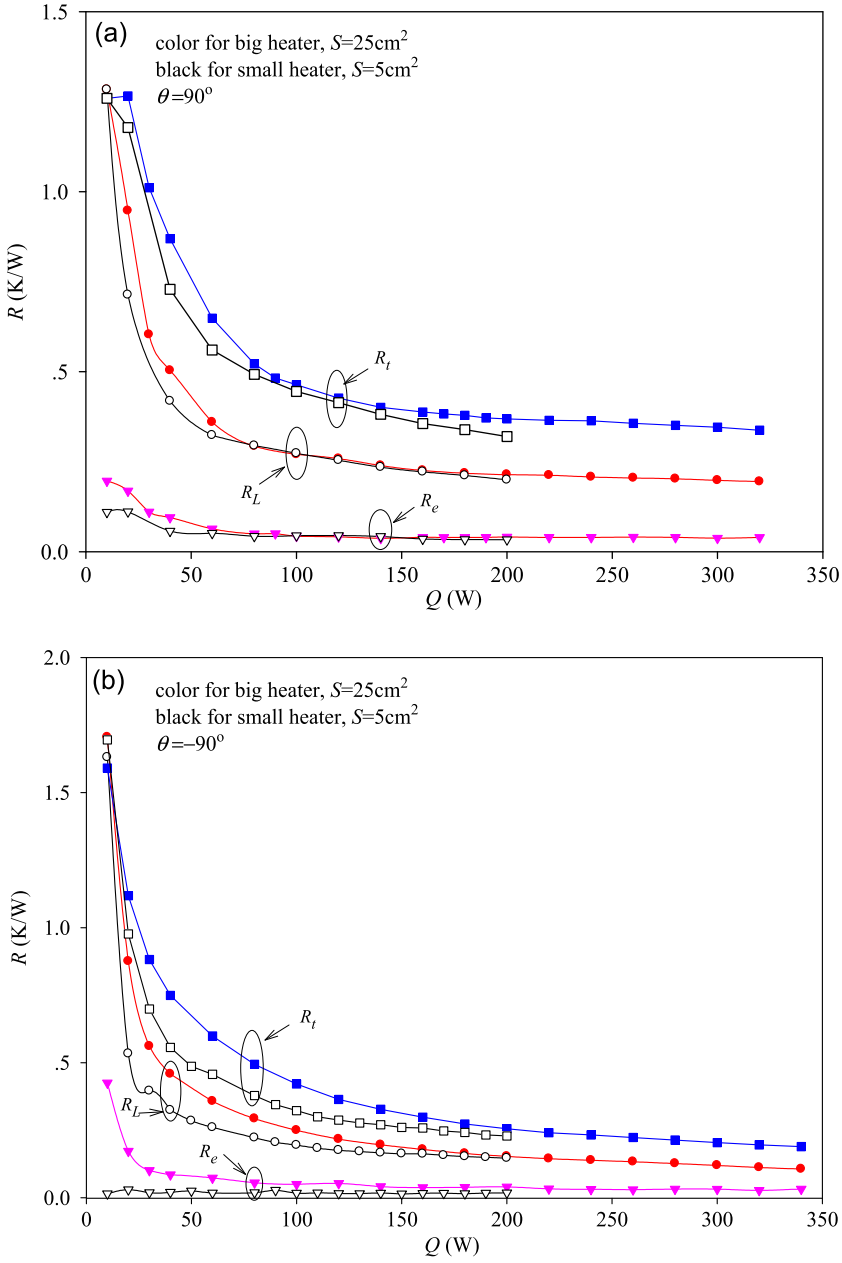

Fig. 12. Effects of heating areas on the thermal resistance: (a) $\theta = -90°$; (b) $\theta = -90°$ (#2–88, $\phi = 51.3\%$, $L_l = 300.0$ mm).

transfer at $\theta = -90°$, while the premise is that there is adequate liquid supply owing to the composite multi-scale porous wicks.

(2) Effects of liquid line length

Fig. 13 shows the effects of liquid line lengths on the thermal resistance for #2–88 at $S = 25$ cm^2. A large length means that the liquid needs to overcome a large resistance to complete a trip from evaporator to compensation chamber. In Fig. 13(a), the liquid line length is the vertical height that the liquid needs to climb in the operation process at $\theta = -90°$, i.e., the so-called anti-gravity height. It is obvious that for three lengths, the thermal resistance decreases with an increase in the heat load, but at the same heat load, the LHP with a larger liquid line length has a larger thermal resistance. For LHP with $L_l = 500.0$ mm, the thermal resistance begins to increase with an increase in the heat load from $Q = 160$ W, indicating that the heat transfer begins to deteriorate. At $\theta = 0°$ (see Fig. 13(b)), although there is no gravity to be overcome, the flow resistance of vapor and liquid increases with an increase of the length at the same heat load, leading to a large thermal resistance. Therefore, the length of the LHP should be reduced as much as possible in practice. In our experiments, the anti-gravity height can reach 500.0 mm, at which the heat load can reach 200 W and still have a good heat transfer performance.

3.3. Critical heat flux

Fig. 14(a) shows the heat flux versus T_C for #1 and #2–88 under different ϕ and θ. Under the same heat flux, the T_C of #2–88 is lower than that of #1 at the corresponding filling ratios. The temperature difference is up to 40 °C at $q = 14.0$ W/cm^2, which indicates that #2–88 has good heat transfer performance. For #1, the CHF is 14.0 W/cm^2 with a T_C of 105 °C at $\phi = 38.5\%$. The CHF increases with an increase in ϕ, which is up to 20.0 W/cm^2 at ϕ

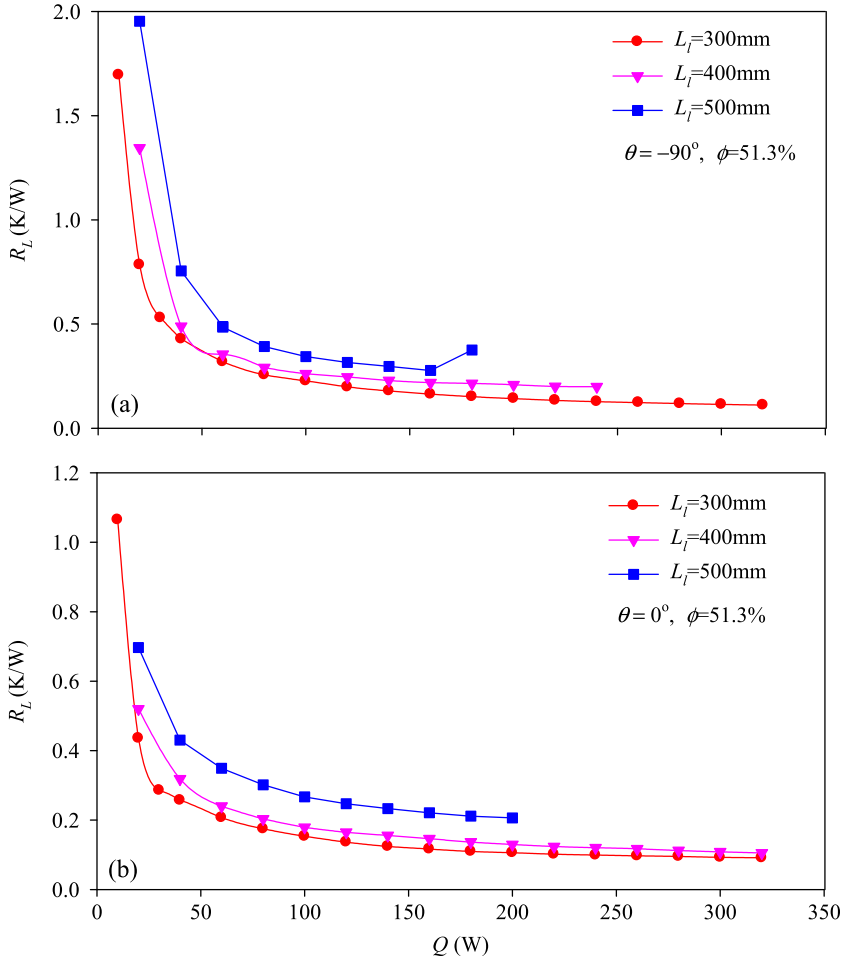

Fig. 13. Effects of liquid line lengths: (a) $\theta = -90°$; (b) $\theta = 0°$ (#2–88, $S = 25\text{cm}^2$).

= 51.3% and 28.0 W/cm^2 at ϕ = 64.1%. Each T_C eventually reaches nearly 100 °C at three ϕ. However, for #2–88, the CHF is 19.0 W/cm^2 with a T_C of 80 °C at ϕ = 38.5%, which is larger than #1 by 5 W/cm^2. On comparing the LHPs with other ϕ, the curve shifts to the left (smaller wall superheat) and the LHP has good heat performance at q < 15 W/cm^2. The optimal ϕ is 51.3% for #2–88, at which the LHP can operate very well in the range of the heat flux from 0 to 40 W/cm^2. However, at ϕ = 64.1%, the heat performance of #2–88 is poorer and the curve shifts to right compared with ϕ = 51.3%. The start-up temperature increases correspondingly by 10 °C. In present experiments, the CHFs of #2–88 at ϕ = 51.3% and ϕ = 64.1% were not obtained because of the limitation of film heaters. The effects of tilt angles can be observed in Fig. 14(b) at ϕ = 51.3%. For #1, the CHFs are 20 W/cm^2, 32 W/cm^2, and 35 W/cm^2 at $\theta = -90°$, 0°, and 90°, respectively. At θ = 90° the CHF is the largest, and the curve shifts to the left at low heat flux, thus indicating that the heat transfer performance is the best at θ = 90° among the three angles at q < 20.0 W/cm^2. On the contrary, for #2–88, all curves shift to the left compared with #1 at the three angles. At $\theta = -90°$ the curve further shifts to left compared with other two angles, which shows that #2–88 has good anti-gravity capacity and it is an important characteristics for our innovative design.

From the viewpoint of flow resistance, the flow of the working fluid within the LHP belongs to vapor-liquid two-phase flow. When the evaporator is heated, the working fluid in the porous wicks evaporates and flows to the condenser. Then, the vapor is condensed into liquid, liquid returns from condenser to evaporator under capillary pressure generated by the porous wick. Therefore, the operation of LHP consists of liquid evaporation, vapor condensation, and the flow of the vapor and the liquid. Capillary pressure (Δp_{cpr}) depends on the pore diameter of wicks and the surface tension of the working fluid. The circulation of the working fluid in the LHP has to overcome all pressure drops. These pressure drops mainly include the flow pressure drop of vapor from the evaporator to the condenser (Δp_v), the flow pressure drop of the liquid from condenser to the evaporator (Δp_l), the pressure drop within the condenser (Δp_{cond}), the pressure drop due to gravity (Δp_g) ($\Delta p_g = \rho g \Delta H$, which might be positive, negative, or zero, where ΔH is the anti-gravity height), and the pressure drop of the liquid and vapor within the porous wicks (Δp_w). If the LHP operates normally, the following equation must be satisfied:

$$\Delta p_{cpr} \geqslant \Delta p_l + \Delta p_v + \Delta p_g + \Delta p_{cond} + \Delta p_w \tag{9}$$

In the practical application, the pressure drop in the liquid line, vapor line, and condenser tube can be decreased by selecting an appropriate pipe diameter. Further, the pressure drop induced by gravity can be reduced by selecting an appropriate tilt angle. Therefore, only the pressure drop of the vapor and the liquid within the porous wicks is focused in this study. If LHP has good heat performance, the capillary pressure would be increased and the pressure drop within the porous wicks would reduce. For conventional LHP, owing to the solid groove wall (see Fig. 4(a)), the area for phase change is small, and the heat needs to go through a long distance to arrive at the porous wick. When the liquid

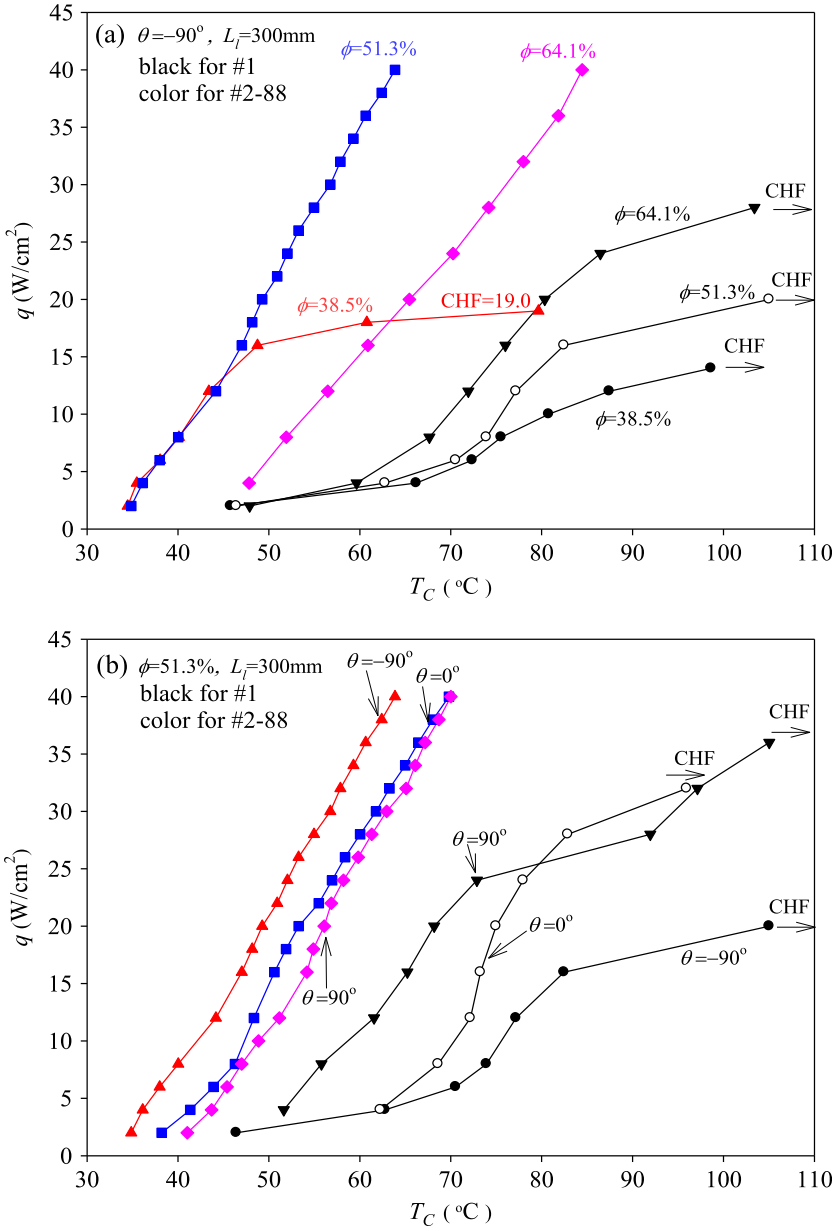

Fig. 14. Heat flux versus evaporator wall center temperature: (a) for different filling ratios; (b) for different tilt angles.

changes into vapor, the vapor needs to turn and then vents into the vapor channel, leading to a conflict with the liquid supply at the phase change region. Although the conventional LHP can separate the flow of vapor and liquid in the vapor channel, it cannot do so successfully in the wicks. However, the LHP with composite wicks, suggested in this study, can solve these problems (see Fig. 4(b)). The phase change takes place not only on the inner surface of evaporator, but also within the groove porous wall in this type of LHP. Thus, the area for phase change is much larger than that in conventional LHP. Besides, the vapor can vent into the vapor channel directly through large pores in the wicks, reducing the flow resistance of the vapor. The liquid also arrive at the phase change region by small pores in the wicks. Thus, the vapor-liquid phase separation is better, and the frictional resistance of vapor-liquid flow is reduced significantly. That is, the composite multiscale porous wicks not only achieve the synergy of pore sizes, taking into account both the liquid supply and vapor release, but also separate the liquid and vapor thoroughly, making them flow in individual paths and reducing the flow resistance greatly.

3.4. Heat leakage

Heat leakage is an important factor affecting the operation of LHP. Large heat leakage reduces the temperature difference between the evaporator and compensation chamber, and thus hinders the circulation of the working fluid or even stops LHP operation. Therefore, a small heat leakage is one of the characteristics of excellent LHP. Fig. 15 shows the heat leakage percentage at different tilt angles. For #2–88, the heat leakage increases with an increase in heat load at low heat load, while the heat leakage begins to decrease at high heat load. The maximum value appears at $Q = 80$ W. The reason can be given as follows: when Q is small, the vapor temperature is low. The temperature difference is small between the evaporator and compensation chamber, which makes LHP have little heat leakage. With increasing Q, the vapor temperature begins to increase. A part of heat can be conducted to the water in the compensation chamber. However, with further increase in Q, the circulation of the working liquid is accelerated. A part of the heat leakage is brought back to the evaporator by

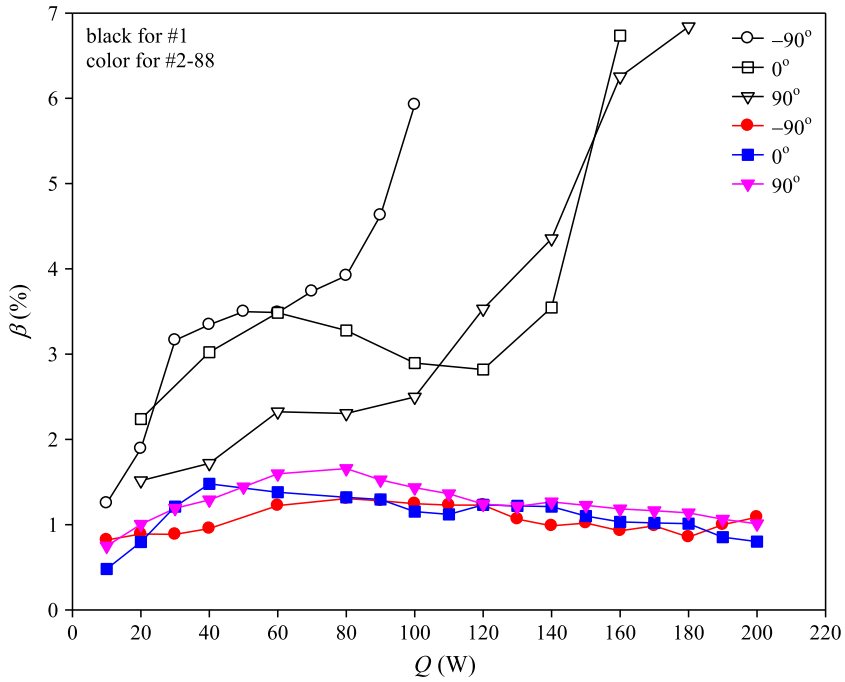

Fig. 15. Heat leakage percentage at different tilt angles.

the liquid flowing from the compensation chamber to the evaporator, thus decreasing the heat leakage.

In addition, as shown in Fig. 15, #2–88 has lower heat leakage than that of #1. At $Q = 90$ W, the heat leakage percentage of #1 is 4.74%, while that of #2–88 is only 1.53%, and the heat leakage is reduced by 67.7%. For #1, the tilt angle has an important effect on the heat leakage. The heat leakage is the smallest at $\theta = 90°$ among the three angles. However, for #2–88, the effects of tilt angles on the heat leakage are not obvious. The heat leakage at $\theta = 90°$ is slightly larger than those at other two angles. The following mechanisms account for the small heat leakage of #2–88: (1) The primary layer wick has a multiscale structure, which allows LHP to achieve a good heat transfer performance. Thus, the heat is mostly absorbed by the working fluid for phase change, and it is carried into the vapor line. Therefore, the heat leakage is small and gives the LHP a positive feedback to enhance heat performance. (2) The third layer wick is made of absorbent wool with excellent thermal insulation. Therefore, composite wicks not only ensure liquid transport, but also effectively prevent heat transfer from the evaporator to the compensation chamber.

From the heat leakage viewpoint, the thermal conductivity of wicks should be as small as possible. However, at the phase change region, it is helpful for liquid evaporation to increase the thermal conductivity of wicks. Thus, this is a contradictory problem. For #2–88, composite wicks with three layers are utilized to achieve high thermal conductivity adjacent to the evaporator wall and high thermal insulation for the whole wicks, realizing a synergy between thermal conductivity and thermal insulation. Therefore, the start-up and heat performance of LHP are improved significantly.

4. Conclusions

LHPs with composite multiscale porous wicks were fabricated innovatively. Heat transfer and start-up characteristics were investigated experimentally for different wick parameters and operating conditions. The conclusions are as follows:

(1) Composite multiscale porous wicks can improve LHP's performance, reduce the start-up time, lower the start-up temperature, and result in only small temperature fluctuations during the start-up process compared with monoporous wicks.

(2) For LHPs with composite multiscale porous wicks, many factors such as liquid filling ratios, heat load, tilt angles, geometric parameters of the porous wicks, and particle size affect the start-up time. In the present study, optimal geometric parameters, which gave the shortest start-up time, were used in the experiments ($w = 1.5$ mm, $p = 1.5$ mm and $h = 1.5$ mm).

(3) In composite multiscale porous wicks, vapor and liquid phases were well separated, and the surface area was enlarged, leading to a successful synergy between vapor release and liquid supply. In particular, the vapor venting requires large vapor channels and large pores to reduce the resistance, and the liquid supply needs small pores to produce a large capillary force. Thus, the composite wicks enable LHP to operate properly under the anti-gravity condition, where the heat flux can reach 40 W/cm^2 without reaching CHF, and T_C is only 63 °C at $Q = 200$ W.

(4) The nucleate boiling and film evaporation regions exist in the operation process from the start-up to high heat flux. In the nucleate boiling region, LHP has a large thermal resistance for a large heating area with the same heat load, while in the film evaporation region, it is less affected by the heating area and more by the heat load.

(5) The LHP with composite wicks solves the contradictory problems and achieves a synergy between thermal conductivity and thermal insulation. The composite wicks ensure not only good thermal conductivity in the primary layer wick, but also good thermal insulation in the entire wick, thus reducing heat leakage from the evaporator to the compensation chamber, which is one of the reasons for the excellent heat performance of LHP. At $Q = 90$ W, the maximum heat leakage can be reduced by 67.7% compared with conventional LHP.

Acknowledgements

This work is supported by the Natural Science Foundation of China (51276061), the Key Project of Natural Science Foundation of China (51436004), and Foundation of CNNC Key Laboratory on Nuclear Reactor Thermal Hydraulics Technology.

References

[1] L.L. Vasiliev, Heat pipes in modern heat exchangers, Appl. Therm. Eng. 25 (2005) 1–19.
[2] K. Nakamura, K. Odagiri, H. Nagano, Study on a loop heat pipe for a long-distance heat transfer under anti-gravity condition, Appl. Therm. Eng. 107 (2016) 167–174.
[3] J.F. Maidanik, S.V. Vershinin, V.F. Kholodov, J.E. Dolgirev, Heat Transfer Apparatus, US patent, No. 4515209, 1985.
[4] Y.F. Maydanik, Loop heat pipes, Appl. Therm. Eng. 25 (2005) 635–657.
[5] S. Launay, V. Sartre, J. Bonjour, Parametric analysis of loop heat pipe operation: a literature review, Int. J. Therm. Sci. 46 (2007) 621–636.
[6] R.R. Riehl, N. Santos, Loop heat pipe performance enhancement using primary wick with circumferential grooves, Appl. Therm. Eng. 28 (2008) 1745–1755.
[7] R. Kempers, D. Ewing, C.Y. Ching, Effect of number of mesh layers and fluid loading on the performance of screen mesh wicked heat pipes, Appl. Therm. Eng. 26 (2006) 589–595.
[8] J.L. Yu, H. Chen, H. Zhao, An experimental investigation on capillary pumped loop with the meshes wick, Int. J. Heat Mass Transfer 50 (2007) 4503–4507.
[9] R.R. Riehl, T. Dutra, Development of an experimental loop heat pipe for application in future space missions, Appl. Therm. Eng. 25 (2005) 101–112.
[10] H. Nagano, H. Nagai, Development of an experimental small loop heat pipe with polytetrafluoroethylene wicks, J. Thermophys. Heat Transfer 25 (2011) 547–552.
[11] L.F. Berti, P.H.D. Santos, E. Bazzo, R. Janssen, D. Hotza, C.R. Rambo, Evaluation of permeability of ceramic wick structures for two phase heat transfer devices, Appl. Therm. Eng. 31 (2011) 1076–1081.
[12] G.P. Celata, M. Cumo, M. Furrer, Experimental tests of a stainless steel loop heat pipe with flat evaporator, Exp. Therm. Fluid Sci. 34 (2010) 866–878.
[13] L. Vasiliev, D. Lossouarn, C. Romestant, A. Alexandre, Y. Bertin, Y. Piatsiushyk, V. Romanenkov, Loop heat pipe for cooling of high-power electronic components, Int. J. Heat Mass Transfer 52 (2009) 301–308.
[14] W.S. Ling, W. Zhou, R.L. Liu, Q.F. Qiu, J. Liu, Thermal performance of loop heat pipe with porous copper fiber sintered sheet as wick structure, Appl. Therm. Eng. 108 (2016) 251–260.
[15] S. Launay, M. Vallée, State-of-the-art experimental studies on loop heat pipes, Frontiers Heat Pipes 2 (2010) 1–27.
[16] E. Meléndez, R. Reyes, The pool boiling heat transfer enhancement from experiments with binary mixtures and porous heating covers, Exp. Therm. Fluid Sci. 30 (2006) 185–192.
[17] M.T. North, D.B. Sarraf, J.H. Rosenfeld, Y.F. Maidanik, S. Vershinin, High heat flux loop heat pipes, in: Proceedings of the Sixth European Symposium on Space Environmental Control Systems, Noordwijk, The Netherlands, 1997, pp. 371–376.
[18] T. Semenic, I. Catton, Experimental study of biporous wicks for high heat flux applications, Int. J. Heat Mass Transfer 52 (2009) 5113–5121.
[19] C.C. Yeh, C.N. Chen, Y.M. Chen, Heat transfer analysis of a loop heat pipe with biporous wicks, Int. J. Heat Mass Transfer 52 (2009) 4426–4434.
[20] F.C. Lin, B.H. Liu, C.T. Huang, Y.M. Chen, Evaporative heat transfer model of a loop heat pipe with bidisperse wick structure, Int. J. Heat Mass Transfer 54 (2011) 4621–4629.
[21] H. Li, Z.C. Liu, B.B. Chen, W. Liu, C. Li, J.G. Yang, Development of biporous wicks for flat-plate loop heat pipe, Exp. Therm. Fluid Sci. 37 (2012) 91–97.
[22] W. Wu, J.H. Du, X.J. Hu, B.X. Wang, Pool boiling heat transfer and simplified one-dimensional model for prediction on coated porous surfaces with vapor channels, Int. J. Heat Mass Transfer 45 (5) (2002) 1117–1125.
[23] D.H. Min, G.S. Hwang, Y. Usta, O.N. Cora, M. Koc, M. Kaviany, 2-D and 3-D modulated porous coatings for enhanced pool boiling, Int. J. Heat Mass Transfer 52 (2009) 2607–2613.
[24] X.B. Ji, J.L. Xu, Z.W. Zhao, W.L. Yang, Pool boiling heat transfer on uniform and non-uniform porous coating surfaces, Exp. Therm. Fluid Sci. 48 (2013) 198–212.
[25] R. Singh, A. Akbarzadeh, M. Mochizuki, Operational characteristics of a miniature loop heat pipe with flat evaporator, Int. J. Therm. Sci. 47 (2008) 1504–1515.
[26] H.X. Zhang, G.P. Lin, T. Ding, X.G. Shao, R.G. Sudakov, Y.F. Maidanik, Experimental study on start-up characteristics of loop heat pipes, Sci. China Ser. E-Eng., Mater. Sci. 48 (2005) 131–144.
[27] B.J. Huang, H.H. Huang, T.L. Liang, System dynamics model and startup behavior of loop heat pipe, Appl. Therm. Eng. 29 (2009) 2999–3005.
[28] D.D. Wang, Z.C. Liu, J. Shen, C. Jiang, B.B. Chen, J.G. Yang, Z.K. Tu, W. Liu, Experimental study of the loop heat pipe with a flat disk-shaped evaporator, Exp. Therm. Fluid Sci. 57 (2014) 157–164.
[29] N.H. Wang, Z. Cui, J. Burger, L. Cheng, Transient behaviors of loop heat pipes for alpha magnetic spectrometer cryocoolers, Appl. Therm. Eng. 68 (2014) 1–9.
[30] W. Joung, T. Yu, J. Lee, Experimental study on the loop heat pipe with a planar bifacial wick structure, Int. J. Heat Mass Transfer 51 (2008) 1573–1581.